Journal of Nuclear Medicine, published on April 17, 2020 as doi:10.2967/jnumed.119.241174

Factors predicting metastatic disease in ^{68}Ga-PSMA-11 PET positive osseous lesions in prostate cancer

Authors: Le Wen Chiu B.S. [1],Courtney Lawhn-Heath M.D.[2], Spencer C. Behr M.D.[2], Roxanna Juarez M.D.[2], Paola M. Perez B.S.[1], Iryna Lobach Ph.D.[3]; Matthew D. Bucknor M.D.[2]; Thomas A. Hope M.D.[2]; Robert R. Flavell M.D., Ph.D[2,4].

Affiliations:

1. University of California San Francisco, School of Medicine

2. University of California San Francisco, Department of Radiology and Biomedical Imaging

3. University of California San Francisco, Department of Epidemiology and Biostatistics

4. University of California San Francisco, Department of Pharmaceutical Chemistry

No conflicts of interest to disclose. Manuscript has been seen and approved by all authors.

Corresponding Author:

Robert Flavell, MD, PhD

Address:

185 Berry Street, Lobby 6, Suite 350

San Francisco, CA 94158

Phone: 917-509-8679

E-mail: robert.flavell@ucsf.edu

First Author:

Le Wen Chiu, B.S.

Address:

50 Kirkham Street

San Francisco, CA 94122

Phone: 562-243-9285

E-mail: lewen.chiu@ucsf.edu

Short title: Guidelines for PSMA PET Interpretation

Word count: 5000

ABSTRACT

Bone is the most common site of distant metastatic spread in prostate adenocarcinoma. Prostate-specific membrane antigen uptake has been described in both benign and malignant bone lesions, which can lead to false-positive findings on ^{68}Ga-prostate-specific membrane antigen-11 positron emission tomography (^{68}Ga-PSMA-11 PET). The purpose of this study was to evaluate the diagnostic accuracy of ^{68}Ga-PSMA-11 PET for osseous prostate cancer metastases and improve bone uptake interpretation using semi-quantitative metrics.

METHODS. 56 prostate cancer patients (18 pre-prostatectomy, 38 biochemical recurrence) who underwent ^{68}Ga-PSMA-11 PET/MRI or PET/CT examinations with osseous PSMA-ligand uptake were included in the study. Medical records were reviewed retrospectively by board-certified nuclear radiologists to determine true or false positivity based on a composite endpoint. For each avid osseous lesion, biological volume, size, PSMA-RADS rating, maximum standardized uptake value (SUVmax), and ratio of lesion SUVmax to liver, blood pool, and background bone SUVmax were measured. Differences between benign and malignant lesions were evaluated for statistical significance, and cut-off values for these parameters were determined to maximize diagnostic accuracy.

RESULTS. Among 56 participants, 13 patients (22.8%) had false-positive osseous ^{68}Ga-PSMA-11 findings and 43 patients (76.8%) had true-positive osseous ^{68}Ga-PSMA-11 findings. Twenty-two patients (39%) had 1 osseous lesion, 18 (32%) had 2-4 lesions, and 16 (29%) had 5 or more lesions. Cut-off values resulting in statistically significant ($p<0.005$) differences between benign and malignant lesions were: PSMA-RADS ≥4, SUVmax ≥4.1, SUVmax ratio of lesion to blood

pool ≥2.11, to liver ≥0.55, and to bone ≥4.4. These measurements corresponded to lesion-based ^{68}Ga-PSMA-11 PET lesion detection rate for malignancy of 80%, 93%, 89%, 21%, 89%, and a specificity of 73%, 73%, 73%, 93%, 60%, respectively.

CONCLUSION. PSMA-RADS rating, SUVmax, and SUVmax ratio of lesion to blood pool can help differentiate benign from malignant lesions on ^{68}Ga-PSMA-11 PET. SUVmax ratio to blood pool above 2.2 is a reasonable parameter to support image interpretation and presented superior lesion detection rate and specificity when compared to visual interpretation by PSMA RADS. These parameters hold clinical value by improving diagnostic accuracy for metastatic prostate cancer on ^{68}Ga-PSMA-11 PET/MRI and PET/CT.

Key words: PSMA PET, prostate cancer, osseous metastasis

INTRODUCTION

Prostate cancer is the most common solid malignancy in men and the third leading cause of cancer-related mortality in the western world (*1*). There is strong emerging evidence to suggest that using positron emission tomography (PET) probes that target prostate-specific membrane antigen (PSMA) can improve diagnostic accuracy and management of patients with prostate cancer (*1-8*). A variety of radiopharmaceuticals including the ^{68}Ga-labelled PSMA inhibitor Glu-NH-CO-NH-Lys(Ahx)-HBED-CC have been widely studied as imaging probes for PET and been shown to increase detection of prostate cancer in patients with biochemical recurrence (*9,10*) and in patients with new diagnosis of prostate cancer (*11*). Although only recently implemented into clinical practice, ^{68}Ga-PSMA PET demonstrated improved sensitivity and specificity compared to traditional imaging modalities such as bone scintigraphy, CT, and MRI in patients with primary intermediate- or high-risk disease (*1,6,12*).

Despite its name, however, PSMA is not solely prostate-specific. It also acts as a folate hydrolase that can be expressed in normal tissues and in both benign and malignant processes (*13,14*). For example, PSMA-ligand uptake can appear in conditions including but not limited to Paget's disease, myelomas, fibrous dysplasia, hemangiomas, and bone fractures (*15-20*), which can represent false-positive findings for metastatic disease on ^{68}Ga-PSMA PET. Given the management implications of the presence of osseous metastatic disease and the potential for false positives, guidelines have been suggested for interpreting ^{68}Ga-PSMA PET osseous lesions, including PSMA-RADS (*21*) and Prostate Cancer Molecular Imaging Standardized Evaluation (*22*). Overall, recent studies suggest a high sensitivity and specificity for bone metastasis using ^{68}Ga-PSMA PET (*20,23*), superior to standard of care imaging including CT or bone scan. The purpose of this study was to evaluate the diagnostic accuracy of ^{68}Ga-PSMA-11 PET findings in

the bone for prostate cancer metastasis and develop a framework for interpretation of these findings in patients with prostate adenocarcinoma.

MATERIALS AND METHODS

Subjects

This study was a secondary analysis of an institutional review board approved prospectively acquired study using ^{68}Ga-PSMA-11 PET, with patient cohorts including those with new diagnosis of prostate cancer and no definitive therapy, and a second cohort of those with biochemical recurrence after definitive treatment (*24,25*). The study (NCT02611882, NCT02919111, NCT02918357, NCT03353740) was performed under an investigational new drug application (IND number 127621), with adjusted validation criteria. Overall, the records of 379 patients with new diagnosis, and 357 patients with biochemical recurrence were reviewed for the mention of abnormal osseous PSMA-ligand uptake in the imaging reports. This yielded a cohort of 56 patients with a history of prostate cancer including 18 patients with new diagnosis, and 38 patients with biochemical recurrence.

PET Image Acquisition and Reconstruction

An ITG germanium-gallium generator and an iQs fluidic labeling module (ITG, Garching/Munich, Germany) were used to prepare ^{68}Ga-PSMA-11 as previously described (*26*). 207.2±55.5 MBq (range 111-355.2 MBq) (5.6±1.5 mCi, range 3.0-9.6 mCi) of ^{68}Ga-PSMA-11 was administered intravenously. After an uptake period of 67±14 minutes (range 46-117 minutes), patients underwent PET/CT (Discovery VCT, GE Healthcare, Waukesha, WI) or PET/MRI (3.0T time-of-flight Signa PET/MRI, GE Healthcare, Waukesha, WI). For patients who underwent PET/CT, a 5-minute acquisition per bed position was used from the pelvis

through the mid abdomen, followed by 3-minute acquisitions from the upper abdomen to the vertex. In the absence of a clinical contraindication, iodinated contrast (Omnipaque 350, 150 cc) was administered to all patients. A diagnostic CT was then obtained and used for both attenuation correction and morphologic evaluation (mA = 240, kV = 120, slice thickness = 2 mm). PET data were processed using iterative reconstruction with four iterations and 14 subsets, matrix size 168 × 168. PET transaxial field of view was 620 mm. Axial PET slice thickness was 5.0 mm.

For patients who underwent PET/MRI, whole body PET and whole body T1 and T2 weighted coronal and axial MRI sequences were acquired simultaneously (3 minutes per bed position). Dedicated imaging of the abdomen/pelvis was also performed (8 minutes per bed position). In the absence of clinical contraindication, gadolinium was administered, and a dynamic contrast enhanced sequence was acquired through the pelvis followed by T2-weighted, diffusion-weighted, and post-contrast delayed T1 weighted imaging (*26*).

Composite Endpoint to Determine True and False Positive Bone Lesions

Bone lesions are not routinely biopsied to determine the presence of metastatic disease. Therefore, a composite endpoint to determine the presence or absence of metastatic disease was developed, outlined on Figs. 1 and 2. Two nuclear radiologists who had undergone 1 year of internship, 4 years of radiology residency, and 1 year of fellowship training in nuclear medicine and who are certified or board-eligible by the American Board of Nuclear Medicine, with 1.5 and 10 years of dedicated nuclear medicine experience evaluated each focus of uptake above the

background level in the bone as a true- or false-positive metastatic lesion. Cross-sectional imaging (CT or MRI) from the ^{68}Ga-PSMA-11 PET was available as an anatomic correlate. An experienced musculoskeletal radiologist with 8 years dedicated experience was consulted to interpret equivocal findings. Benign and malignant lesions were differentiated based on accepted criteria on anatomic CT or MRI imaging (*27*).

Gallium-68-Labeled Prostate-Specific Membrane Antigen PET Image Analysis

All images were reviewed in separate sessions by two other nuclear radiologists, with 1 and 9 years of dedicated nuclear medicine experience who were blinded to the true or false positive determination above. Lesions were judged qualitatively by PSMA RADS and quantitatively by several SUV metrics, measured separately by both readers. Discrepancies in lesion determination were resolved by consensus.

Statistical Analysis

Sample characteristics were summarized by age, prior treatment, PSA level at the time of imaging, anatomical correlate, and Gleason score at diagnosis. Cut-off values for key parameters were inferred based on the Youden index (*28*). Area Under the ROC curve (AUC) and 95% deLong Confidence Interval, which assess the stability of the AUC estimate, were used to evaluate the ability of key parameters to determine diagnoses. Variable and location differences between benign and malignant lesions were calculated using Student's t-test and Fisher's exact test. P-values <0.05 were considered statistically significant. Interrater reliability was evaluated with the Cohen kappa statistic, and strength of agreement was determined according to the definition described by Landis and Koch (*29*).

RESULTS

Patient Population

Of 736 patients who underwent ^{68}Ga-PSMA PET/CT or PET/MRI, 56 patients had abnormal PSMA-ligand uptake in the bones and qualified for this study (Fig. 1). Demographics of this study population are summarized in Table 1.

Determination of True and False Positivity by Composite Endpoint

A composite endpoint, outlined in Fig. 2, was used to determine if ^{68}Ga-PSMA PET findings were true positive (i.e. metastasis) or false positive. Thirteen of 56 patients (23.2%) were determined to have false-positive lesions and forty-three of 56 patients (72.8%) were determined to have true-positive lesions. Forty true-positive lesions were determined by the multiplicity seen on PET/CT or PET/MRI or the confirmatory or follow-up imaging. One patient was considered having a true-positive lesion due to changes on follow-up imaging and a PSA response after radiation to the metastasis (Fig. 3A). Three patients had pathologic correlation, wherein biopsy of the lesion revealed metastatic prostate cancer (Fig. 3B). Thirteen false-positive lesions were determined by confirmatory imaging or imaging follow-up, and subsequent stability on imaging for at least one year without definitive treatment. Two patients had their PSA drop to zero after prostatectomy, and were considered as having false-positive lesions (Fig. 4). In contrast, one patient had a PSA that continued to rise after radiation therapy to a solitary lesion, which was considered false-positive (Supplemental Fig. 1). Diagnoses for false-positive lesions are included in Table 2.

^{68}Ga-PSMA-11 PET Image Analysis, Detection Rate, and Uptake

Nineteen lesions were found in the ribs, 48 in the vertebrae, 30 in the pelvis, 12 in other appendicular regions, and 1 in the calvarium. There was no significant difference between the rate of true- and false-positive lesions by anatomic location (Supplemental Fig. 2). Among true positive lesions, 15.8% (15/95) were found in the ribs, 42.1% (40/95) in the vertebrae, 29.5% (28/95) in the pelvis, 11.6% (11/95) in other appendicular locations, and 1% (1/95) in the calvarium. Among false positive lesions, 26.7% (4/15) were found in the ribs, 53.3% (8/15) in the vertebrae, 13.3% (2/15) in the pelvis, 6.7% (1/15) in other appendicular locations, and 0% (0/15) in the calvarium.

Diagnostic accuracy by patient- and lesion-based analysis is shown in Table 3. Optimal cut-off values determined by ROC AUC analysis to differentiate metastases from benign lesions in a patient-based analysis were SUVmax ≥4.4 (95% confidence interval (CI): [0.70, 0.99]), and SUVmax ratio to blood pool ≥2.2 (95% CI: [0.67, 0.99]), to liver ≥1.33 (95% CI: [0.62, 0.99]), and to bone ≥7.11 (95% CI: [0.74, 0.98]), biological volume ≥0.62 cm^3 (95% CI: [0.35, 0.71]), size ≥1.8 cm (95% CI: [0.41, 0.83]), and PSMA RADS ≥4 (95% CI: [0.65, 0.96]). Optimal cut-off values in a lesion-based analysis were SUVmax ≥4.1 (95% CI: [0.69, 0.96]), and SUVmax ratio to reference to blood pool ≥2.11 (95% CI: [0.69, 0.96]), to liver ≥0.55 (95% CI: [0.62, 0.91]), and to bone ≥4.4 (95% CI: [0.71, 0.94]), biological volume ≥0.52 cm^3 (95% CI: [0.36, 0.68]), size ≥1.8 cm (95% CI: [0.35, 0.75]), and PSMA RADS ≥4 (95% CI: [0.66, 0.94]). ROC curves and AUC results are shown in Supplemental Figs. 3 and 4.

Patient- and lesion-based PSMA RADS ratings for total lesions had almost perfect interrater reliability (Table 4).

No statistical differences were found in mean size or biological volume between benign and malignant lesions, in both a patient- and lesion-based comparison (Supplemental Tables 1 and 2). In contrast, differences in means of lesion SUVmax, SUVmax ratios to blood pool, liver, bone, and PSMA RADS rating between benign and malignant lesions were statistically significant (p<0.005), in both a patient- and lesion-based comparison.

DISCUSSION

This study was performed as a secondary analysis of patients who underwent a ^{68}Ga-PSMA-11 PET/CT or PET/MR under a prospective research protocol. The goal of this study was to ascertain the diagnostic accuracy of this technique to detect osseous metastases. The substantial percentage of patients whose lesions were determined as true or false positives for metastatic disease based on confirmatory or follow-up imaging suggests that simultaneous CT or MR imaging is crucial for interpretation of ^{68}Ga-PSMA-11 PET.

Our study confirms the high diagnostic accuracy of SUVmax and PSMA-RADS to distinguish between metastases and benign lesions that are PSMA-avid on ^{68}Ga-PSMA-11 PET/MRI and PET/CT. Among the parameters evaluated, SUVmax appears to be the most accurate and reliable PET parameter, with a statistically superior lesion detection rate, specificity, positive predictive value, and negative predictive value (Fig. 5). This conclusion is consistent with a prior analysis of bone lesions in DOTA TOC PET in neuroendocrine tumors, and also in similar analyses of PSMA-ligand uptake in primary prostate lesions and in mediastinal lymph nodes (*30,31*). Moreover, since SUVmax is easily measured, it is a particularly useful parameter in characterizing lesions as malignant or benign in clinical practice.

A review of the independent factors and development of a combined model for analysis was not performed here. Therefore, this study cannot conclude that SUV parameters are helpful for visually equivocal findings only. Our results complement the existing literature supporting the accuracy of ^{68}Ga-PSMA-11 PET to stage prostate cancer bone metastasis and its superiority to conventional imaging such as bone scan, CT, or MRI alone (*20,32*).

Limitations

This study has a several limitations. Firstly, this study used patient data from a single center, introducing selection bias contingent on the particular patient population of this center. It is important to note that the lesion detection rate and specificity of ^{68}Ga-PSMA-11 PET/CT or MRI cannot be reasonably differentiated from the 736 patients to start with and 56 to enter the study. Future studies should include larger cohorts, as the present study is limited by the small sample size and lack of prospective validation. Moreover, patients were identified for study inclusion via retrospective review of the radiology reports, which may result in some patients not being included due to osseous lesions being missed on initial review. Secondly, this study used only a single radiopharmaceutical, ^{68}Ga-PSMA-11, whereas a multiplicity of tracers is currently under investigation. Prior studies have demonstrated different true and false positive findings based on the agents, with a notably higher false positive rate of ^{18}F-PSMA-1007 when compared against ^{68}Ga-PSMA-11 (*30,33*). Importantly, the presented findings are likely not relevant for ^{18}F-ligands. Finally, cut-off values of the various measured parameters of ^{68}Ga-PSMA-11 uptake to differentiate between true- and false-positive lesions for metastatic disease was determined by Youden's index.

CONCLUSION

Consideration of SUVmax, SUVmax ratio to blood pool, and PSMA RADS ratings of osseous lesions observed on ^{68}Ga-PSMA-11 PET enables high diagnostic accuracy for detecting prostate cancer osseous metastases. The current study demonstrates the importance of considering these parameters when interpreting equivocal findings on ^{68}Ga-PSMA-11 PET, along with the corresponding CT or MRI anatomic correlate. In particular, SUVmax ratio to blood pool above 2.2 appears to be a reasonable parameter to support image interpretation, given the difficult reproducibility of ^{68}Ga-SUVmax across different scanners. SUVmax ratio to blood pool presented superior lesion detection rate, specificity, positive predictive value, and negative predictive value when compared to visual interpretation by PSMA RADS. These findings establish criteria for radiological interpretation of ^{68}Ga-PSMA PET in order to direct timely diagnosis and clinical management of patients with metastatic prostate cancer in the bone.

Conflicts of Interest and Disclosures:

This study was institutionally funded by the UCSF Summer Explore grant. No other potential conflicts of interest relevant to this article exist.

Key Points:

QUESTION: Which imaging findings are predictive of a true prostate cancer osseous metastasis?

PERTINENT FINDINGS: This is a retrospective cohort study of 56 prostate cancer patients, pre-prostatectomy or with biochemical recurrence, in a single-center who underwent ^{68}Ga-PSMA-11 PET/CT or PET/MRI. Based on our analysis, radiological interpretation with consideration of SUVmax, PSMA RADS rating, and anatomical correlates is essential for improving the

diagnostic accuracy of ^{68}Ga-PSMA PET to detect prostate cancer metastasis to the bone. SUVmax ratio to blood pool above 2.2 is a reasonable parameter to support image interpretation and presented superior lesion detection rate, specificity, positive predictive value, and negative predictive value when compared to visual interpretation by PSMA RADS.

IMPLICATIONS FOR PATIENT CARE: Improved accuracy when interpreting ^{68}Ga-PSMA PET scans affects the timely and appropriate clinical management of patients with prostate cancer that has metastasized to the bone and can furthermore augment patient satisfaction and healthcare savings by avoiding unnecessary treatment based on false positive findings.

REFERENCES

1. Hirmas N, Al-Ibraheem A, Herrmann K, et al. [68Ga]PSMA PET/CT improves initial staging and management plan of patients with high-risk prostate cancer. *Mol Imaging Biol*. 2019;21:574–581.
2. Uprimny C, Kroiss AS, Decristoforo C, et al. ^{68}Ga-PSMA-11 PET/CT in primary staging of prostate cancer: PSA and Gleason score predict the intensity of tracer accumulation in the primary tumour. *Eur J Nucl Med Mol Imaging*. 2017;44:941-949.
3. Zacho HD, Nielsen JB, Afshar-Oromieh A, et al. Prospective comparison of 68Ga-PSMA PET/CT, 18F-sodium fluoride PET/CT and diffusion weighted-MRI at for the detection of bone metastases in biochemically recurrent prostate cancer. *Eur J of Nucl Med Mol Imaging.* 2018;45:1884-1897.
4. Pyka T, Okamoto S, Dahlbender M, et al. Comparison of bone scintigraphy and 68Ga-PSMA PET for skeletal staging in prostate cancer. *Eur J of Nucl Med Mol Imaging.* 2016;43:2114-2121.
5. Maurer T, Gschwend JE, Rauscher I, et al. Diagnostic efficacy of (68)Gallium-PSMA positron emission tomography compared to conventional imaging for lymph node staging in 130 consecutive patients with intermediate to high risk prostate cancer. *J Urol*. 2016;195:1436-1443.
6. van Leeuwen PJ, Emmett L, Ho B, et al. Prospective evaluation of 68Gallium-prostate-specific membrane antigen positron emission tomography/computed tomography for preoperative lymph node staging in prostate cancer. *BJU Int.* 2017;119:209-215.

7. Fendler WP, Calais J, Eiber M, et al. Assessment of 68Ga-PSMA-11 PET accuracy in localizing recurrent prostate cancer: a prospective single-arm clinical trial. *JAMA Oncol.* 2019;5:856-863.
8. Sterzing F, Kratochwil C, Fiedler H, et al. (68)Ga-PSMA-11 PET/CT: a new technique with high potential for the radiotherapeutic management of prostate cancer patients. *Eur J of Nucl Med Mol Imaging.* 2016;43:34-41.
9. Maurer T, Eiber M, Schwaiger M, Gschwend JE. Current use of PSMA–PET in prostate cancer management. *Nat Rev Urology*. 2016;13:226–235.
10. Uprimny C, Kroiss AS, Fritz J, et al. Early PET imaging with [68]Ga-PSMA-11 increases the detection rate of local recurrence in prostate cancer patients with biochemical recurrence. *Eur J of Nucl Med Mol Imaging*. 2017;44:1647-1655.
11. Budäus L, Leyh-Bannurah SR, Salomon G, et al. Initial experience of 68Ga-PSMA PET/CT imaging in high-risk prostate cancer patients prior to radical prostatectomy. *Eur Urol.* 2016;69:393-396.
12. Lengana T, Lawal IO, Boshomane TG, et al. 68Ga-PSMA PET/CT replacing bone scan in the initial staging of skeletal metastasis in prostate cancer: a fait accompli? *Clin Genitourin Cancer.* 2018;16:392-401.
13. Hofman MS, Hicks RJ, Maurer T, Eiber M. Prostate-specific membrane antigen PET: clinical utility in prostate cancer, normal patterns, pearls, and pitfalls. *RadioGraphics*. 2018;38:200–217.
14. Pianou NK, Stavrou PZ, Vlontzou E, Rondogianni P, Exarhos DN, Datseris IE. More advantages in detecting bone and soft tissue metastases from prostate cancer using 18F-PSMA PET/CT. *Hell J Nucl Med*. 2019;22:6-9.

15. Artigas C, Alexiou J, Garcia C, et al. Paget bone disease demonstrated on (68)Ga-PSMA ligand PET/CT. *Eur J of Nucl Med Mol Imaging.* 2016;43:195-196.
16. Sasikumar A, Joy A, Pillai MR, Nanabala R, Thomas B. 68Ga-PSMA PET/CT imaging in multiple myeloma. *Clin Nucl Med.* 2017;42:e126-e127.
17. De Coster L, Sciot R, Everaerts W, et al. Fibrous dysplasia mimicking bone metastasis on 68GA-PSMA PET/MRI. *Eur J of Nucl Med Mol Imaging.* 2017;44:1607-1608.
18. Artigas C, Otte FX, Lemort M, van Velthoven R, Flamen P. Vertebral hemangioma mimicking bone metastasis in 68Ga-PSMA ligand PET/CT. *Clin Nucl Med.* 2017;42:368-370.
19. Jochumsen MR, Dias AH, Bouchelouche K. Benign traumatic rib fracture: a potential pitfall on 68Ga-prostate-specific membrane antigen PET/CT for prostate cancer. *Clin Nucl Med.* 2018;43:38-40.
20. Zacho HD, Nielsen JB, Haberkorn U, Stenholt L, Petersen LJ. 68Ga-PSMA PET/CT for the detection of bone metastases in prostate cancer: a systematic review of the published literature. *Clin Physiol Funct Imaging*. 2017;38:911–922.
21. Rowe SP, Pienta KJ, Pomper MG, Gorin MA. Proposal for a structured reporting system for prostate-specific membrane antigen–targeted PET imaging: PSMA-RADS version 1.0. *J Nucl Med.* 2018;59:479-485.
22. Eiber M, Herrmann K, Calais J, et al. Prostate cancer molecular imaging standardized evaluation (PROMISE): proposed miTNM classification for the interpretation of PSMA-ligand PET/CT. *J Nucl Med.* 2018;59:469-478.

23. Pomykala KL, Czernin J, Grogan TR, Armstrong WR, Williams J, Calais J. Total-body 68Ga-PSMA-11 PET/CT for bone metastasis detection in prostate cancer patients: Potential impact on bone scan guidelines. *J Nucl Med*. 2019 [Epub ahead of print].
24. Hope TA, Aggarwal R, Chee B, et al. Impact of 68Ga-PSMA-11 PET on management in patients with biochemically recurrent prostate cancer. *J Nucl Med.* 2017;58:1956-1961.
25. Lawhn-Heath C, Flavell RR, Behr SC, et al. Single-center prospective evaluation of 68Ga-PSMA-11 PET in biochemical recurrence of prostate cancer. *AJR Am J Roentgenol.* 2019;213:266-274.
26. Lake ST, Greene KL, Westphalen AC, et al. Optimal MRI sequences for 68Ga-PSMA-11 PET/MRI in evaluation of biochemically recurrent prostate cancer. EJNMMI Res. 2017;7:77.
27. Hakim DN, Pelly T, Kulendran M, Caris JA. Benign tumours of the bone: A review. *J Bone Oncol.* 2015;4:37-41.
28. Habibzadeh F, Habibzadeh P, Yadollahie M. On determining the most appropriate test cut-off value: the case of tests with continuous results. *Biochem Med (Zagreb)*. 2016;26:297–307.
29. Landis JR, Koch GG. The measurement of observer agreement for categorical data. *Biometrics.* 1977;33:159–174.
30. Kuten J, Fahoum I, Savin Z, et al. Head-to head comparison of 68Ga-PSMA-11 with 18F-PSMA-1007 PET/CT in staging prostate cancer using histopathology and immunohistochemical analysis as reference-standard. *J Nucl Med.* 2019 [Epub ahead of print].

31. Afshar-Oromieh A, Sattler LP, Steiger K, et al. Tracer uptake in mediastinal and paraaortal thoracic lymph nodes as a potential pitfall in image interpretation of PSMA ligand PET/CT. *Eur J Nucl Med Mol Imaging*. 2018;45:1179-1187.
32. Sachpedkidis C, Eder M, Kopka K, et al. (68)Ga-PSMA-11 dynamic PET/CT imaging in biochemical relapse of prostate cancer. *Eur J of Nucl Med Mol Imaging.* 2016;43:1288-1299.
33. Rauscher I, Krönke M, Horn T, Weber WA, Eiber M. Frequency of PET-positive benign findings on PSMA-ligand PET/CT: matched-pair comparison of 68Ga-PSMA-11 and 18F-PSMA-1007. *Nuklearmedizin*. 2019;58:176.

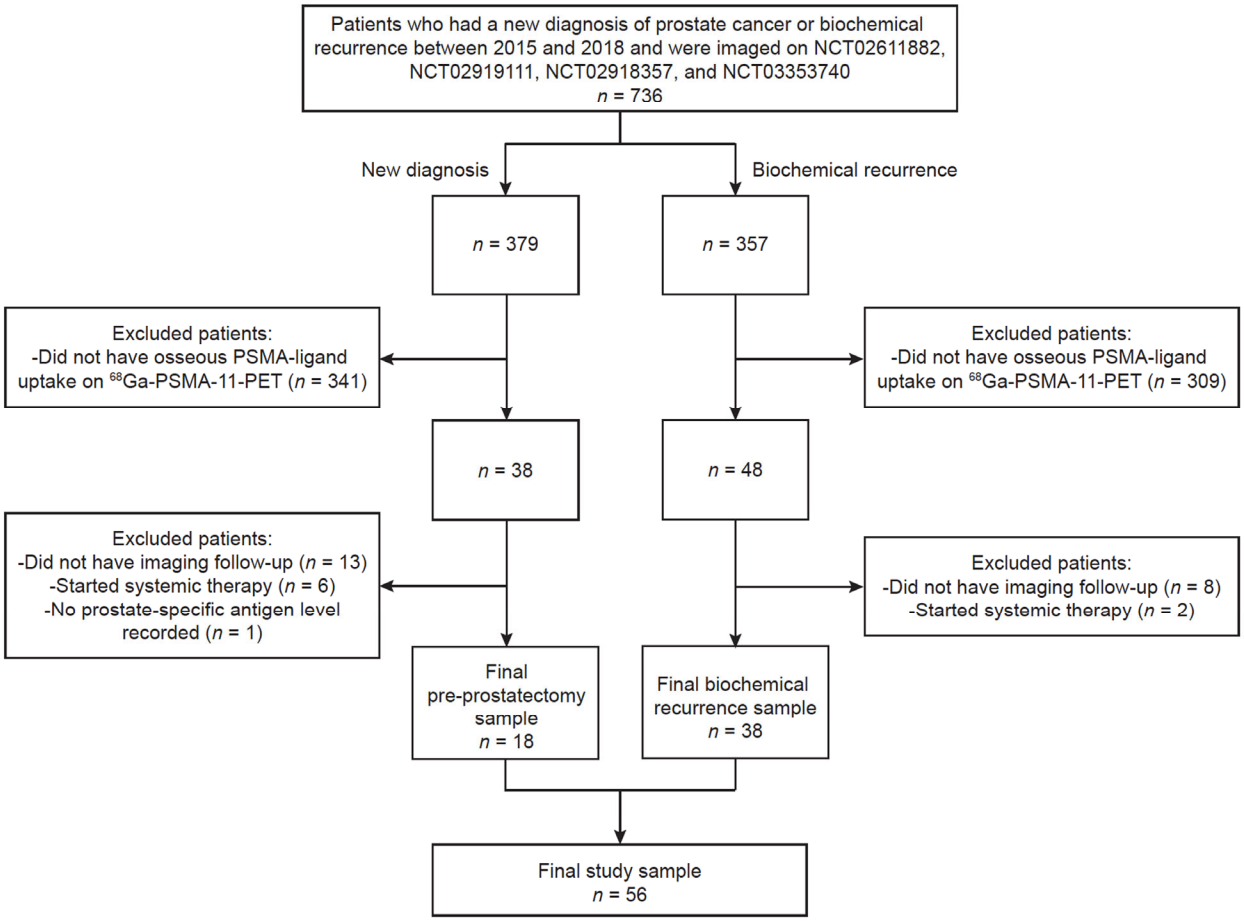

FIGURE 1: Flowchart shows inclusion and exclusion criteria by which pre-prostatectomy patients and patients who had biochemical recurrence of prostate cancer were selected for this study. Number of patients qualifying under each criterion is noted. PSMA: prostate-specific membrane antigen; PET: positron emission tomography

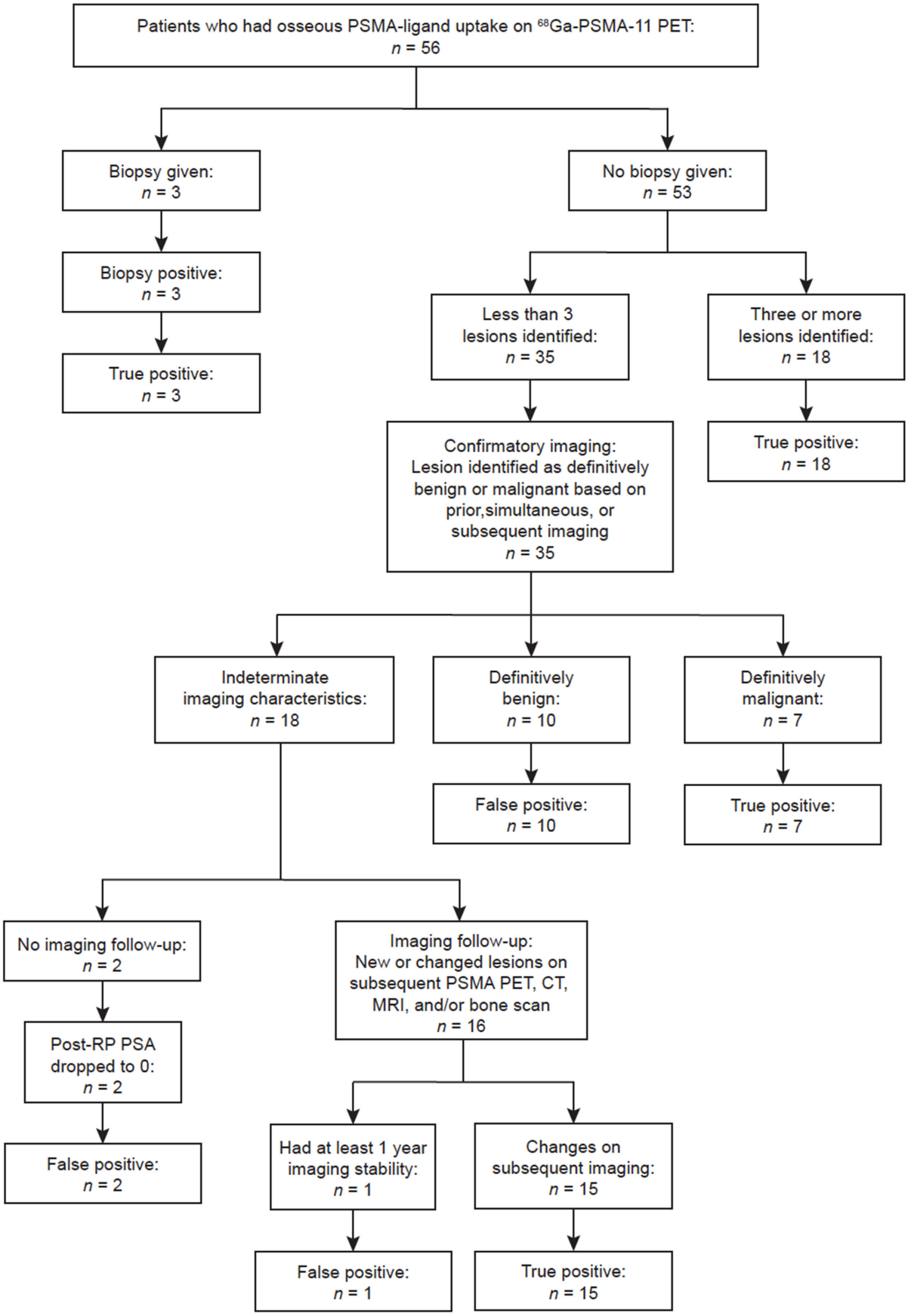
Patients who had osseous PSMA-ligand uptake on 68Ga-PSMA-11 PET: n = 56
Biopsy given: n = 3
No biopsy given: n = 53
Biopsy positive: n = 3
True positive: n = 3
Less than 3 lesions identified: n = 35
Three or more lesions identified: n = 18
True positive: n = 18
Confirmatory imaging: Lesion identified as definitively benign or malignant based on prior,simultaneous, or subsequent imaging n = 35
Indeterminate imaging characteristics: n = 18
Definitively benign: n = 10
Definitively malignant: n = 7
False positive: n = 10
True positive: n = 7
No imaging follow-up: n = 2
Imaging follow-up: New or changed lesions on subsequent PSMA PET, CT, MRI, and/or bone scan n = 16
Post-RP PSA dropped to 0: n = 2
False positive: n = 2
Had at least 1 year imaging stability: n = 1
Changes on subsequent imaging: n = 15
False positive: n = 1
True positive: n = 15

FIGURE 2: Flowchart shows the process of patient-based lesion validation in this study of pre-prostatectomy patients and patients with biochemical recurrence of prostate cancer. Number of patients qualifying under each criterion is noted. In total, 43 patients had validated true positive lesions and 13 had false positive lesions. In the case of multiple lesions with PSMA-ligand uptake, lesions were considered to be true positive lesions if one lesion was determined to be true positive. True and false positive bone findings on imaging are aimed to be confirmed by biopsy if clinically feasible, multiplicity of lesions, imaging follow-up, or drop in prostate-specific antigen level.

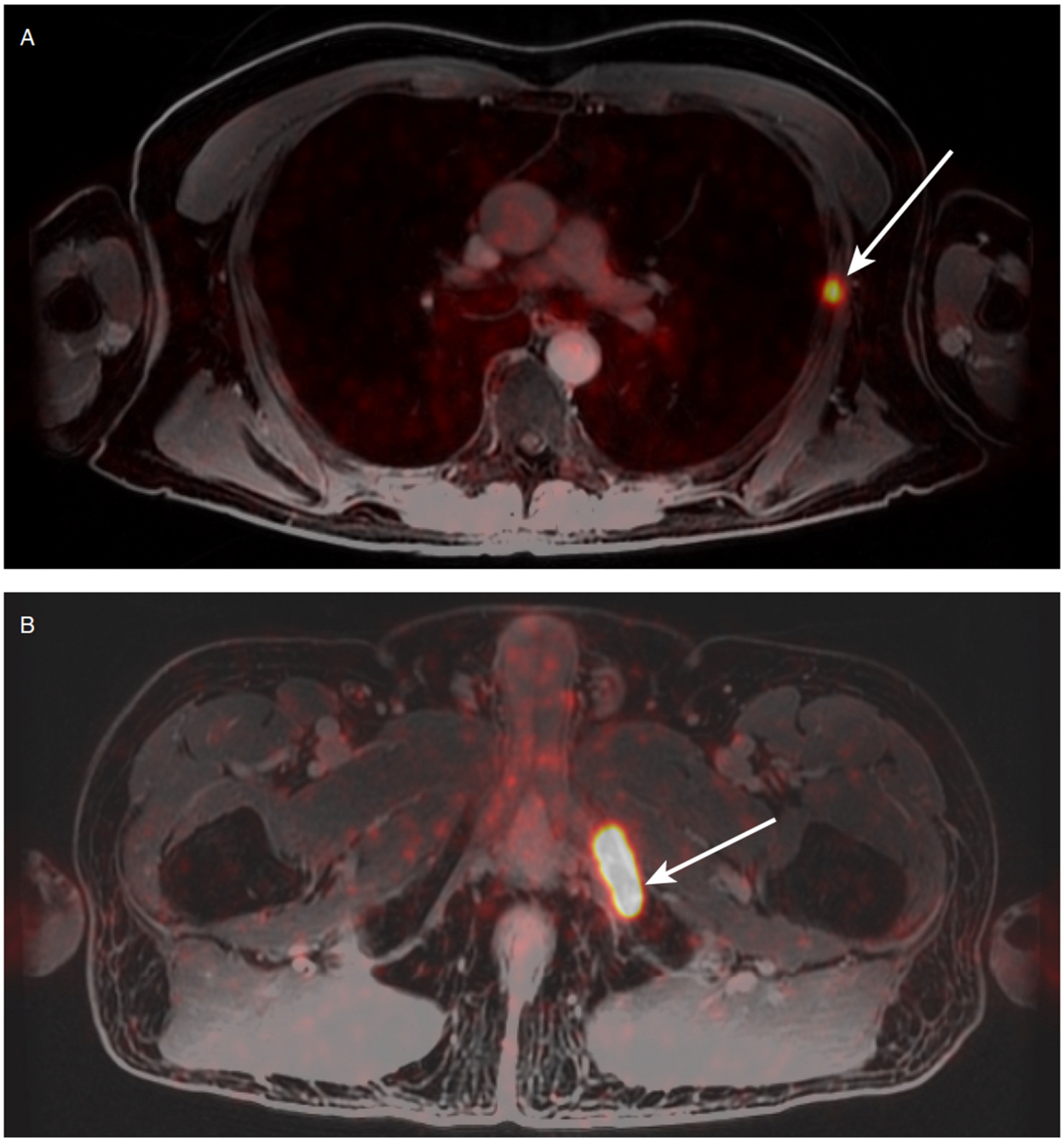

FIGURE 3: Examples of true positive findings

A) 76-year-old male with biochemical recurrence of prostate cancer. Axial ^{68}Ga-PSMA-11 fused PET/MR image shows abnormal radiotracer uptake within the left lateral sixth rib (arrow). PSA levels trended down post-stereotactic body radiation therapy treatment to the rib. Lesion was considered true-positive.

B) 66-year-old male with biochemical recurrence of prostate cancer. Axial ^{68}Ga PSMA-11 fused PET/MR image shows abnormal radiotracer uptake within the left pubic bone (arrow). Subsequent biopsy of the left inferior pubic ramus revealed metastatic prostate cancer. Lesion was considered true-positive.

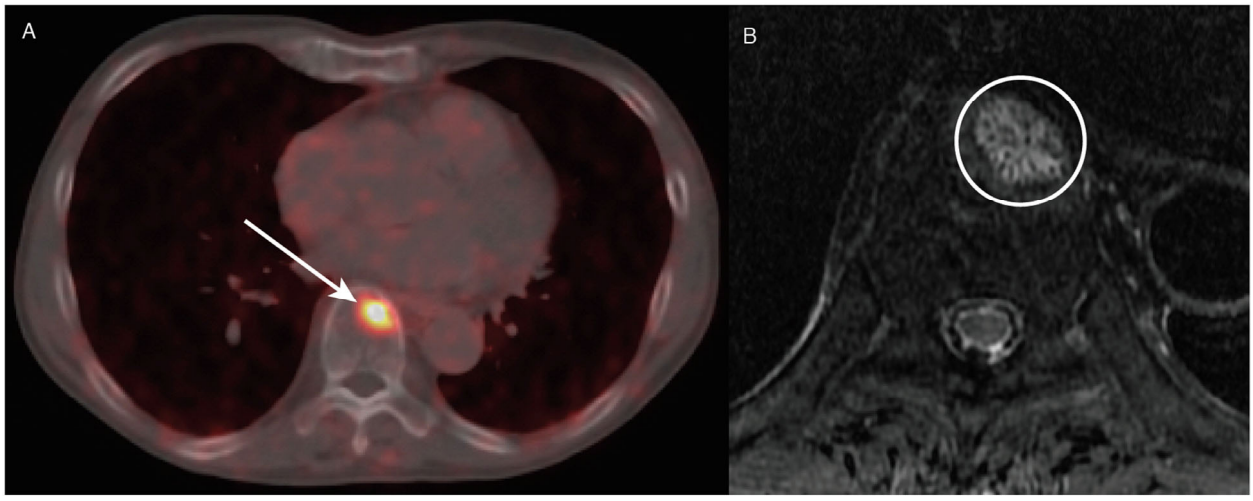

FIGURE 4: Example of false positive findings

75-year-old male with prostate cancer, pre-prostatectomy, whose PSA dropped to 0 post-prostatectomy.

A) Axial ^{86}Ga-labeled prostate-specific membrane antigen fused PET/CT image shows abnormal radiotracer uptake within the T9 vertebral body (arrow).

B) Axial T2 weighted magnetic resonance image through the T9 vertebral body demonstrates a high T2 signal lesion with a trabeculated marrow appearance (circle). Findings suggest a diagnosis of atypical hemangioma.

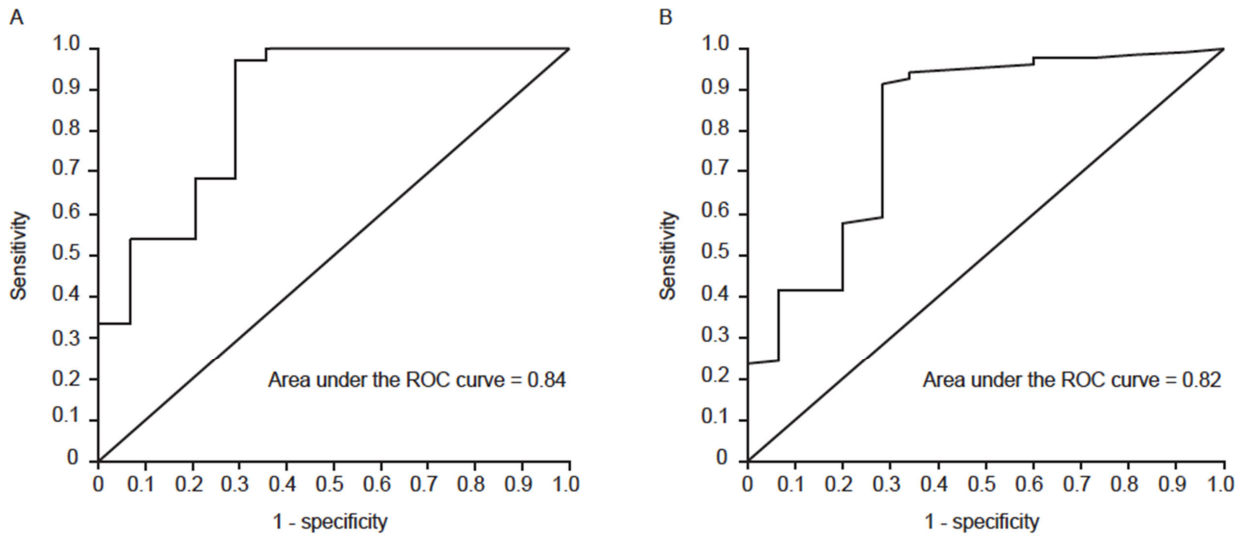

FIGURE 5:

A) Patient-based receiver operating characteristic (ROC) curve for the SUV max of PSMA-avid osseous lesions (n=54; n=13 false positive lesions and n=41 true positive lesions). Area under the curve (AUC)=0.84, 95% Confidence Interval (0.70, 0.99).

B) Lesion-based receiver operating characteristic (ROC) curve for the SUV max of PSMA-avid osseous lesions (n=107; n=15 false positive lesions and n=92 true positive lesions). AUC=0.82, 95% Confidence Interval (0.69, 0.96).

TABLE 1: Clinical characteristics of study sample

Characteristic	Value
Number of patients	56
Mean age (range, SD)	67.0 (48-78, ±7.9)
Prior treatment (%)†	
Radical prostatectomy	10 (13)
Prostate bed radiation	9 (11)
Metastasis-directed radiation	4 (5)
Both radical prostatectomy and radiation therapy	14 (18)
Androgen deprivation therapy or chemotherapy	28 (35)
Other, unknown	9 (11)
Currently undergoing androgen deprivation therapy or chemotherapy	6 (8)
Median PSA level (range)	13.7 (0.05-132.5)
PET/MR (%)	40 (71)
PET/CT (%)	16 (29)
Gleason score at diagnosis (%)	
3+3	5 (9)
3+4	8 (14)
4+3	8 (14)
4+4	12 (21)
4+5	13 (23)
5+4	5 (9)
5+5	2 (4)
N/A	3 (5)
PSMA PET findings:	
Bone lesions:	
1 lesion	22 (39)
2-4 lesions (oligometastatic)	18 (32)
5+ lesions	16 (29)
True positive bone disease	43 (77)
False positive bone disease	13 (23)
Lymph nodes:	
None	26 (46)
Pelvic only	13 (23)
Nonregional only	6 (11)
Pelvic and nonregional	11 (20)
Other sites of metastatic disease	0 (0)

*SD = standard deviation, PSA = prostate-specific antigen, PET = positron emission tomography, MR = magnetic resonance, CT = computed tomography. Data are expressed as numbers followed by range, standard deviation, or percentages in parentheses as indicated.

†Prior treatment % only applies to patients with biochemical recurrence.

TABLE 2: Diagnoses of false positive lesions

Diagnosis	Pre-prostatectomy	Biochemical recurrence
Hemangioma	2	1
Paget's disease	1	0
Venous plexus	1	0
Degenerative	1	1
Indeterminate	5	4

*The degenerative diagnosis includes degenerative disc disease and degenerative changes. Lesions for which no diagnosis was given were categorized as indeterminate.

TABLE 3: Diagnostic accuracy of PET parameters to detect osseous metastases

Characteristic	Cut off	Se [CI] *n*	Sp [CI] *n*	PPV [CI] *n*	NPV [CI] *n*
Patient-based analysis					
SUV_{max}	≥ 4.4	98% [0.87, 1.0] *n* = 54	62% [0.32, 0.86] *n* = 54	91% [0.78, 0.97] *n* = 54	90% [0.55, 1.0] *n* = 54
SUV_{max} ratio					
To blood pool	≥ 2.2	97% [0.87, 1.0] *n* = 53	69% [0.39, 0.91] *n* = 53	91% [0.78, 0.97] *n* = 53	90% [0.55, 1.0] *n* = 53
To liver	≥ 1.33	78% [0.62, 0.89] *n* = 53	77% [0.46, 0.95] *n* = 53	91% [0.76, 0.98] *n* = 53	53% [0.29, 0.76] *n* = 53
To bone	≥ 7.11	100% [0.91, 1.0] *n* = 53	31% [0.09, 0.61] *n* = 53	82% [0.68, 0.91] *n* = 53	100% [0.40, 1.0] *n* = 53
Biological volume	≥ 0.62	93% [0.80, 0.98] *n* = 53	23% [0.05, 0.54] *n* = 53	79% [0.64, 0.89] *n* = 53	50% [0.12, 0.88] *n* = 53
Size	≥ 1.8	50% [0.33, 0.67] *n* = 48	80% [0.44, 0.97] *n* = 48	90% [0.70, 0.99] *n* = 48	30% [0.14, 0.50] *n* = 48
PSMA RADS	≥ 4	93% [0.80, 0.98] *n* = 53	69% [0.39, 0.91] *n* = 53	90% [0.77, 0.97] *n* = 53	75% [0.43, 0.95] *n* = 53
Lesion-based analysis					
SUV_{max}	≥ 4.1	93% [0.86, 0.98] *n* = 107	73% [0.45, 0.92] *n* = 107	96% [0.89, 0.99] *n* = 107	65% [0.38, 0.86] *n* = 107
SUV_{max} ratio					
To blood pool	≥ 2.11	89% [0.80, 0.94] *n* = 104	73% [0.45, 0.92] *n* = 104	95% [0.88, 0.99] *n* = 104	52% [0.30, 0.74] *n* = 104
To liver	≥ 0.55	21% [0.13, 0.31] *n* = 104	93% [0.68, 1.0] *n* = 104	95% [0.75, 1.0] *n* = 104	17% [0.09, 0.26] *n* = 104
To bone	≥ 4.4	89% [0.80, 0.94] *n* = 104	60% [0.32, 0.84] *n* = 104	93% [0.85, 0.97] *n* = 104	47% [0.24, 0.71] *n* = 104
Biological volume	≥ 0.52	89% [0.81, 0.95] *n* = 98	21% [0.05, 0.51] *n* = 98	87% [0.78, 0.93] *n* = 98	25% [0.05, 0.57] *n* = 98
Size	≥ 1.8	39% [0.28, 0.51] *n* = 85	80% [0.44, 0.97] *n* = 85	94% [0.79, 0.99] *n* = 85	15% [0.07, 0.27] *n* = 85
PSMA RADS	≥ 4	80% [0.70, 0.88] *n* = 104	73% [0.45, 0.92] *n* = 104	95% [0.87, 0.99] *n* = 104	38% [0.21, 0.58] *n* = 104

*PET = positron emission tomography, Se = sensitivity, Sp = specificity, PPV = positive predictive value, NPV = negative predictive value, CI = confidence interval.

†Units for size are in centimeters, where a clearly measurable lesion was present on anatomic imaging.

‡SUV could not be accurately quantified in n = 2 cases due to technical error.

TABLE 4: PSMA RADS interrater reliability

Group	κ
Patient-based PSMA RADS rating for lesions with PSMA-ligand uptake	0.88
Lesion-based PSMA RADS rating for lesions with PSMA-ligand uptake	0.82

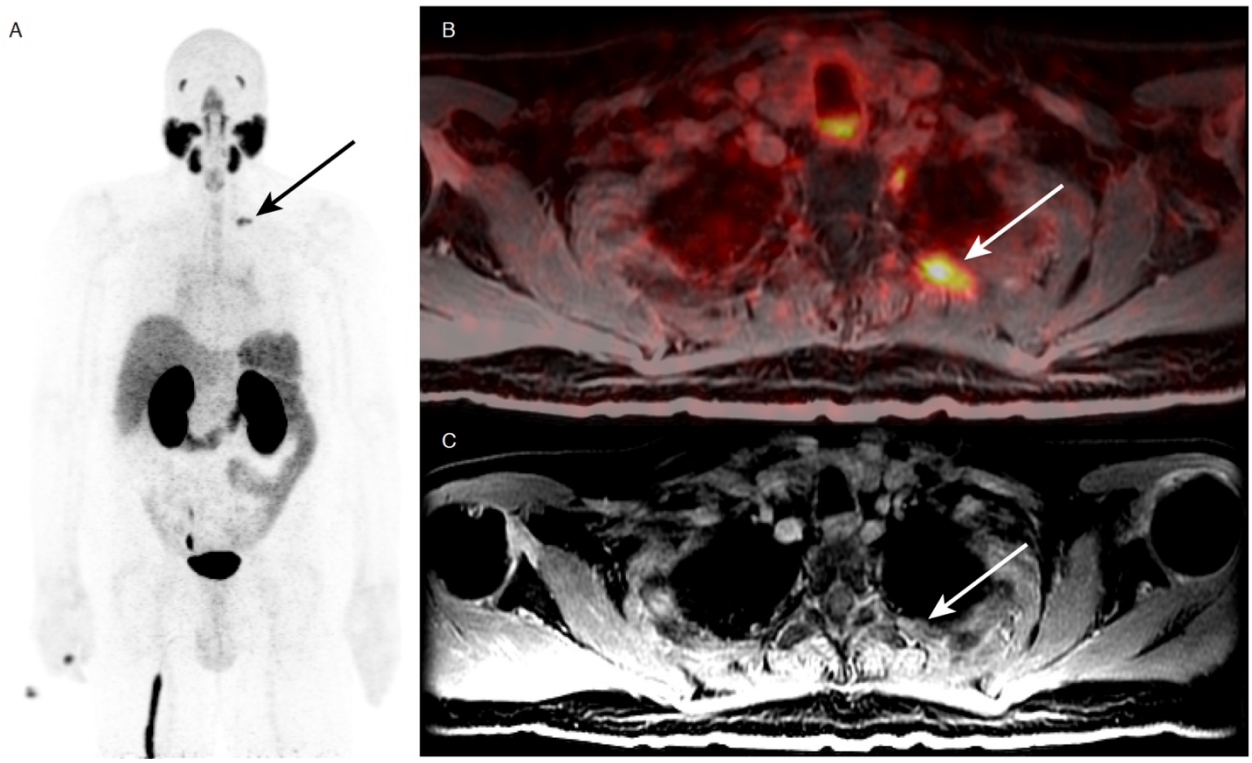

Supplemental Figure 1: 73-year-old male with a history of prostate cancer and PSA of 1.37 at the time of the scan. ^{68}Ga-PSMA PET/MRI (A, B) demonstrates a solitary rib lesion with associated contrast enhancement on MRI (C). The patient underwent stereotactic body radiotherapy to the lesion; however, PSA continued to climb despite radiation therapy. Findings were considered a false positive.

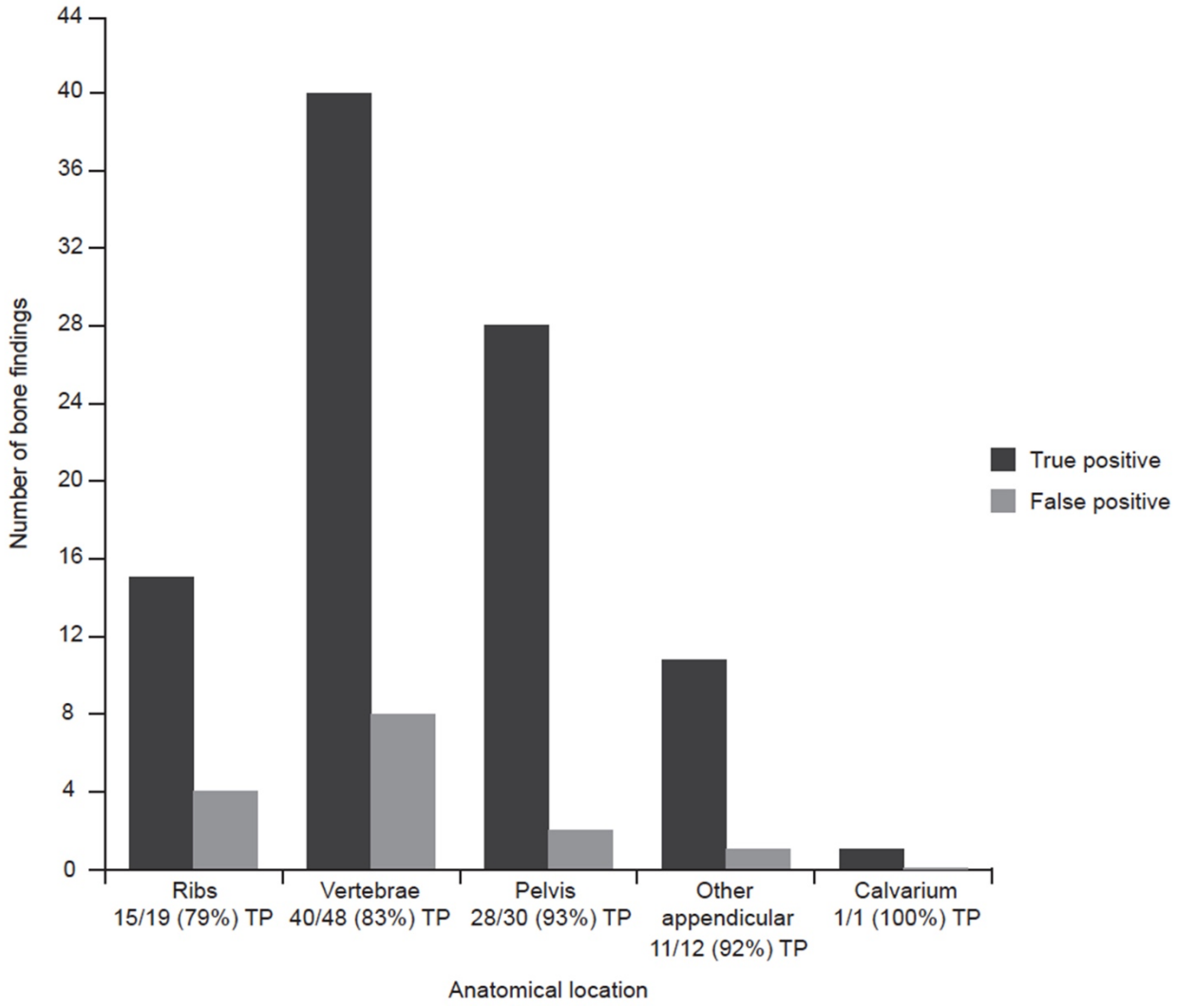

Supplemental Figure 2: Anatomical locations of PSMA-avid lesions between true and false positives for prostate cancer metastases. Other appendicular locations include the humerus, femoral neck, lesser trochanter, sternum, scapula, clavicle, and glenoid. No statistically significant difference was found between the proportions of true and false positive lesions identified at each location ($p>0.05$).

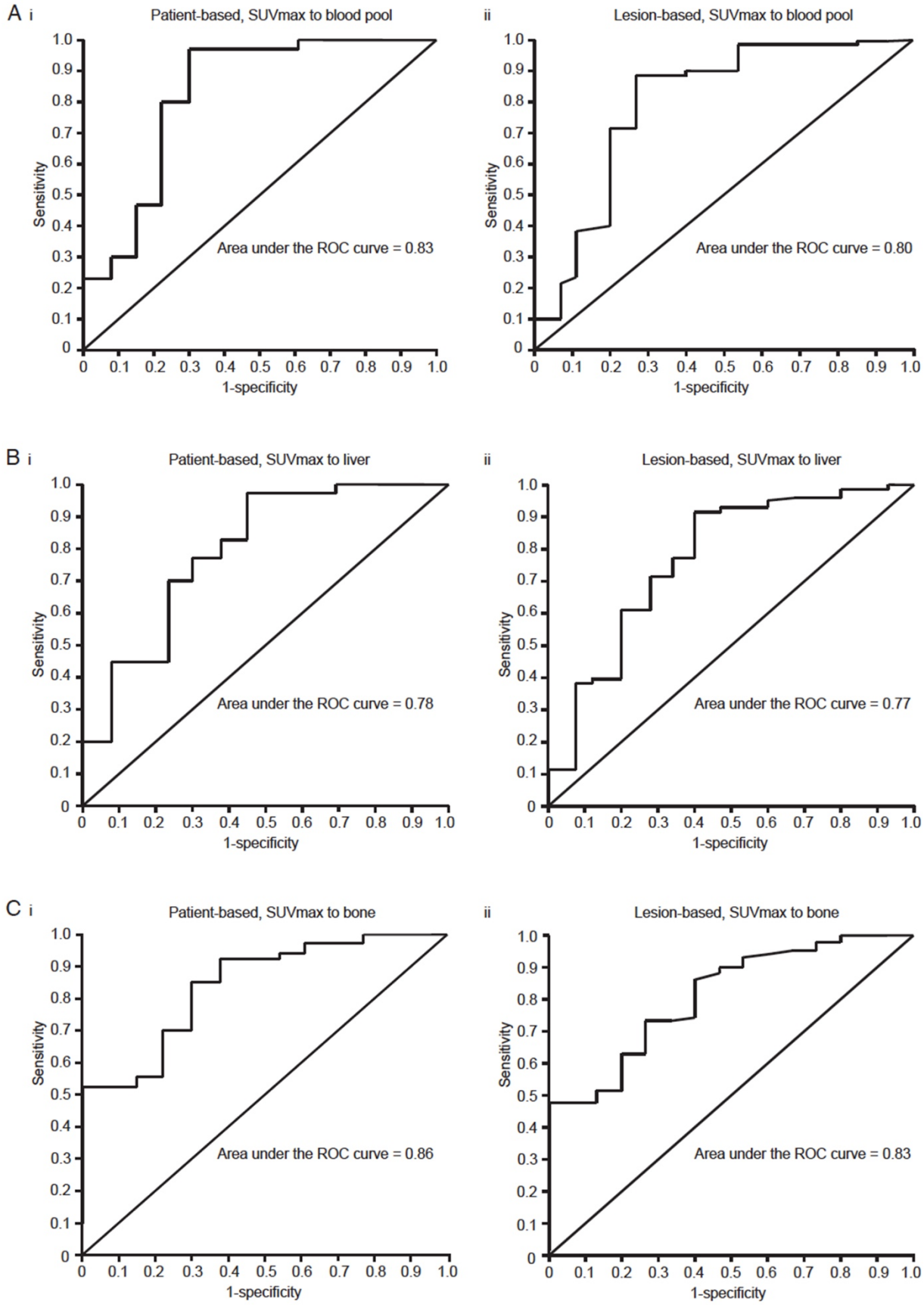
A i
Patient-based, SUVmax to blood pool
Sensitivity
1-specificity
Area under the ROC curve = 0.83
ii
Lesion-based, SUVmax to blood pool
Sensitivity
1-specificity
Area under the ROC curve = 0.80
B i
Patient-based, SUVmax to liver
Sensitivity
1-specificity
Area under the ROC curve = 0.78
ii
Lesion-based, SUVmax to liver
Sensitivity
1-specificity
Area under the ROC curve = 0.77
C i
Patient-based, SUVmax to bone
Sensitivity
1-specificity
Area under the ROC curve = 0.86
ii
Lesion-based, SUVmax to bone
Sensitivity
1-specificity
Area under the ROC curve = 0.83

Supplemental Figure 3: Receiver operating characteristic (ROC) curves for SUVmax to reference organs

A) i. Patient-based ROC curve for SUVmax ratio to blood pool (n=53; n=13 patients with false positive lesions and n=40 patients with true positive lesions).
   ii. Lesion-based ROC curve for SUVmax ratio to blood pool (n=104; n=15 patients with false positive lesions and n=89 patients with true positive lesions).

B) i. Patient-based ROC curve for SUVmax ratio to liver (n=53; n=13 patients with false positive lesions and n=40 patients with true positive lesions).
   ii. Lesion-based ROC curve for SUVmax ratio to liver (n=104; n=15 patients with false positive lesions and n=89 patients with true positive lesions).

C) i. Patient-based ROC curve for SUVmax ratio to bone (n=53; n=13 patients with false positive lesions and n=40 patients with true positive lesions).
   ii. Lesion-based ROC curve for SUVmax ratio to bone (n=104; n=15 patients with false positive lesions and n=89 patients with true positive lesions).

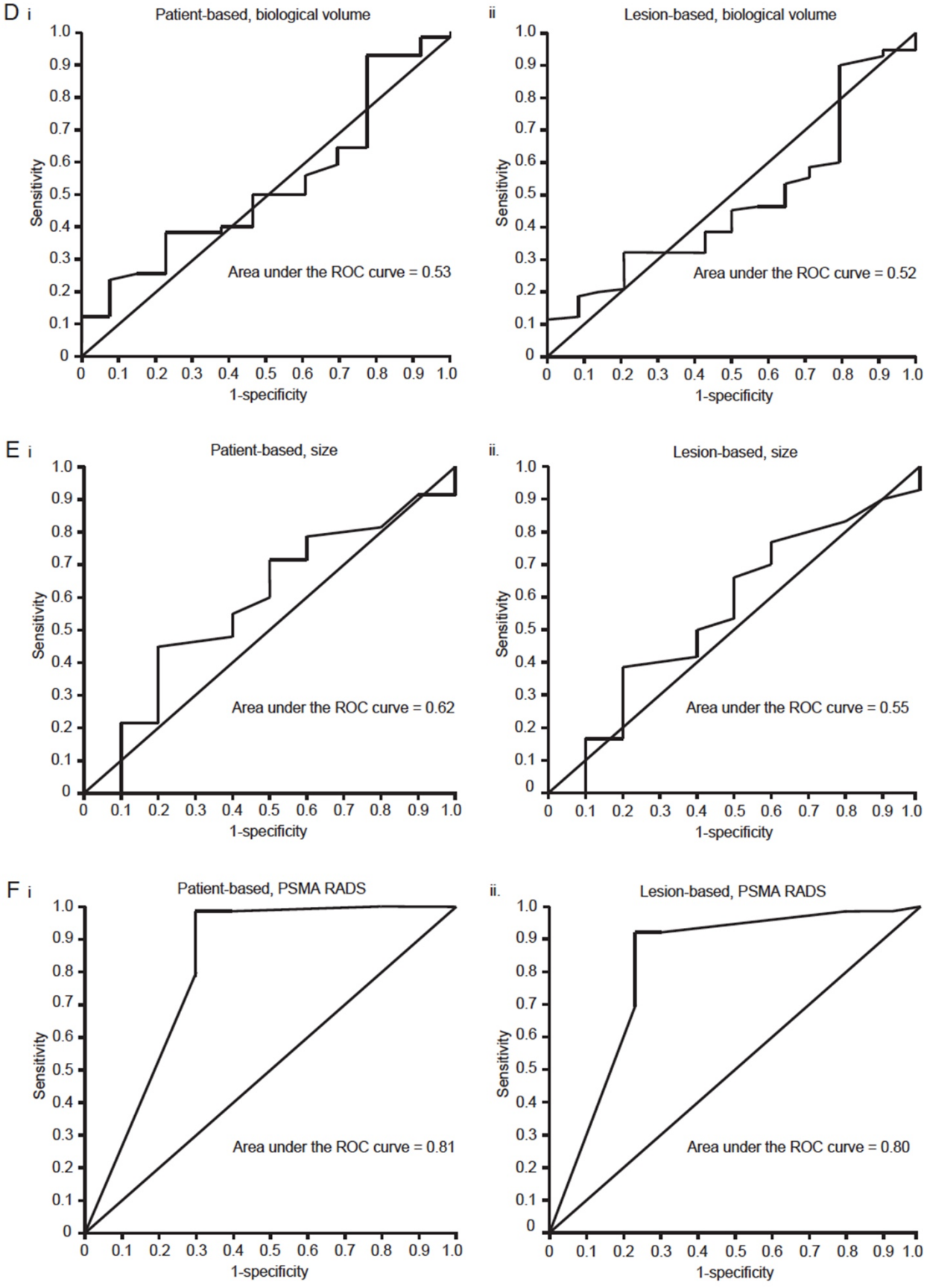
D i
Patient-based, biological volume
Sensitivity
1-specificity
Area under the ROC curve = 0.53
ii
Lesion-based, biological volume
Sensitivity
1-specificity
Area under the ROC curve = 0.52
E i
Patient-based, size
Sensitivity
1-specificity
Area under the ROC curve = 0.62
ii.
Lesion-based, size
Sensitivity
1-specificity
Area under the ROC curve = 0.55
F i
Patient-based, PSMA RADS
Sensitivity
1-specificity
Area under the ROC curve = 0.81
ii.
Lesion-based, PSMA RADS
Sensitivity
1-specificity
Area under the ROC curve = 0.80

Supplemental Figure 4: Receiver operating characteristic (ROC) curves for biological volume and size of lesions

D) i. Patient-based ROC curve for biological volume of lesions (n=55; n=13 patients with false positive lesions and n=42 patients with true positive lesions).
ii. Lesion-based ROC curve for biological volume of lesions (n=98; n=14 patients with false positive lesions and n=84 patients with true positive lesions).

E) i. Patient-based ROC curve for lesion size (n=48; n=10 patients with false positive lesions and n=38 patients with true positive lesions).
ii. Lesion-based ROC curve for lesion size (n=85; n=10 patients with false positive lesions and n=75 patients with true positive lesions).

F) i. Patient-based ROC curve for PSMA RADS rating of lesions (n=53; n=13 patients with false positive lesions and n=40 patients with true positive lesions).
ii. Lesion-based ROC curve for PSMA RADS rating of lesions (n=92; n=15 false positive lesions and n=77 true positive lesions).

Supplemental Table 1**:** Patient-based comparison of benign and metastatic lesions

Parameter	**Mean of benign lesions** **Range** **n**	**Mean of malignant lesions** **Range** **n**	**Significance**
SUV_{max}	6.61 1.4-27.1	23.98 3.7-96	$p<0.001$
SUV_{max} ratio to blood pool	4.31 0.73-18.07	12.15 1.55-80.4	$p=0.004$
SUV_{max} ratio to liver	1.23 0.05-5.21	3.21 0.51-14.4	$p=0.003$
SUV_{max} ratio to bone	5.74 1.0-14.3	28.22 2.67-195	$p<0.001$
Biological volume	2.58 0.39-8.9	4.72 0.22-30	$p=0.099$
Size	2.12 0.8-8.6	1.98 0.5-6.0	$p=0.863$
PSMA RADS	3 2-5	5 3B-5	$p<0.001$

Supplemental Table 2: Lesion-based comparison of benign and metastatic lesions

Parameter	Mean of benign lesions Range n	Mean of malignant lesions Range n	Significance
SUV_{max}	6.35 1.4-27.1	17.65 1.6-78	$p<0.001$
SUV_{max} ratio to blood pool	3.90 0.73-18.07	9.41 0.76-80.4	$p=0.003$
SUV_{max} ratio to liver	1.11 0.05-5.21	2.60 0.25-14.4	$p=0.002$
SUV_{max} ratio to bone	5.53 1.0-14.3	28.22 1.78-195	$p<0.001$
Biological volume	2.62 0.39-8.9	3.58 0.16-30	$p=0.261$
Size	2.12 0.8-8.6	2.01 0.5-7.7	$p=0.885$
PSMA RADS	3B 2-5	5 2-5	$p<0.001$